Supporting Information

Batra et al. 10.1073/pnas.1112235108

SI Text

SI Materials and Methods. ***Crystallization of Pol β substrate complexes.*** Binary complex crystals with 8-oxoG as the template base in a 1-nucleotide gapped DNA were grown (1). The sequence of the template strand (16-mer) with 8-oxoG (underlined) in the template (coding) position was 5′- CCG ACG TCG CAT CAG C- 3′. The primer strand (10-mer) sequence was 5′- GCT GAT GCG A -3′. The downstream oligonucleotide (5-mer) was phosphorylated, and the sequence was 5′- GTC CC—3′. The binary complex crystals were then soaked in artificial mother liquor (50 mM imidazole, pH 7.5, 20% PEG3350, 90 mM sodium acetate, 200 mM $MgCl_2$ with nonhydrolyzable dNTP analogs [5 mM dAMP(CH_2)PP or dCMP(CF_2)PP] and 12% ethylene glycol as cryoprotectant. This resulted in ternary complex crystals. The sequence of the template strand with 8-oxoG at the n-1 position was: 5′- CCG ACG GCG CAT CAG C- 3′. The primer strand (10-mer) sequences was 5′- GCT GAT GCG A/C -3′. Annealing with the primer strand created the 8-oxoG:A or 8-oxoG:C base pairs at the template-primer terminus. The template base in the single-nucleotide gap in both cases was unmodified G and the downstream oligonucleotide was as described above. Binary complex crystals were grown under similar conditions as described above. These crystals were then soaked in artificial mother liquor (50 mM imidazole, pH 7.5, 20% PEG3350, 90 mM sodium acetate, 200 mM $MgCl_2$) with a nonhydrolyzable dCTP analog [5 mM dCMP(CF_2)PP] and 12% ethylene glycol as cryoprotectant, resulting in ternary complex crystals. Diffraction quality data also were collected for the binary complex crystals as described.

Data collection and structure determination. Data were collected at 100 K on a CCD detector system mounted on a MiraMax®-007HF (Rigaku Corporation) rotating anode generator. Data were integrated and reduced with HKL2000 software (2). Ternary complex structures were determined by molecular replacement with reference to a previously determined structure of pol β complexed with one-nucleotide gapped DNA and incoming dUMPNPP [Protein Data Bank (PDB) ID code 2FMS) (1). The new crystal structures have similar lattices as the reference structure and are sufficiently isomorphous to determine the molecular-replacement model using CNS and manual model building using O. The figures were prepared in Chimera (3).

Kinetic assays. A 34-mer oligonucleotide DNA substrate containing a one-nucleotide gap was prepared by annealing 3 gel-purified oligonucleotides to create the one-nucleotide gap at position 16. Each oligonucleotide was resuspended in 10 mM Tris-HCl, pH 7.4, and 1 mM EDTA, and the concentration was determined from their UV absorbance at 260 nm. The annealing reactions were carried out in a PCR thermocycler by incubating a solution of 10 μM primer with 12 μM each of downstream and template oligonucleotides at 95 °C for 5 min followed by 30 min at 65 °C, and then slow cooling (1 °C/ min) to 10 °C. The sequence of the gapped DNA substrate was: primer, 5′-CTG CAG CTG ATG CG(C or A)-3′, downstream oligonucleotide, 5′-GTA CGG ATC CCC GGG TAC-3′, and template, 3′-GAC GTC GAC TAC GCG GCA TGC CTA GGG GCC CAT G-5′ (the underlined nucleotide represents the template guanine opposite the primer terminus that is substituted with 8-oxoG where indicated). The primer was 5′-labeled with [γ-^{32}P]ATP using Optikinase (USB Corp.) and the free radioactive ATP was removed with Biospin 6 columns. The downstream oligonucleotide was synthesized with a 5′-phosphate.

Steady-state kinetic parameters for dCTP insertion opposite guanine in a one-nucleotide DNA gap were determined by initial velocity measurements as described previously (4). Enzyme activities were determined using a standard reaction mixture (20 μL) containing 50 mM Tris-HCl, pH 7.4, 100 mM KCl, 5 mM $MgCl_2$, and 200 nM one-nucleotide gapped DNA. Enzyme concentrations and reaction time intervals were chosen so that substrate depletion or product inhibition did not influence initial velocity measurements. Reactions were stopped with 20 μL of 0.3 M EDTA and mixed with an equal volume of formamide dye, and the products separated on 15% denaturing polyacrylamide gels. The dried gels were analyzed by phosphorimagery to quantify product formation.

SI Discussion. The dual coding potential of the 8-oxoG base lesion in DNA is discussed in the main text and illustrated in the diagram in Fig. S1*A*. The *syn*-conformation and *anti*-conformations of 8-oxoG are stabilized in the respective base pairs with A and C, respectively (5). The base excision repair (BER) pathway for removal of 8-oxoG from genomic DNA has been referred to as a component of the "GO system" (6). In the diagram shown in Fig. S1*B*, unrepaired 8-oxoG can lead to the G to T transversion mutation. In mammalian systems, BER counteracts this mutagenesis by removal of the 8-oxoG base from the 8-oxoG:C base pair and the A base from the 8-oxoG:A base pair, as illustrated. Subsequently, gap-filling DNA synthesis by pol β along with other BER steps restores the DNA or facilitates G to T mutagenesis.

Various DNA polymerases have been characterized for catalytic efficiency of insertion opposite the 8-oxoG template base, and representative results are summarized in Table S1. The preference for error-free insertion of dCTP vs. mutagenic bypass insertion of dATP varies by several orders of magnitude among the polymerases from different families and sources, indicating that the polymerase and/or reaction conditions, such as sequence context around 8-oxoG, play an active role in the coding potential of 8-oxoG. Pol β has only a twofold preference for dCTP insertion over dATP insertion.

Properties of the binary complex crystal structure not shown in Fig. 1. As discussed in the main text and illustrated here in Fig. S2*A*, the enzyme is in the open conformation and very similar to the enzyme in the reference binary complex structure (7) (PDB ID code 3ISB). The DNA component (i.e., single-nucleotide gapped DNA with 8-oxoG in the template base position) of the binary complex is shown in Fig. S2*B*. The illustration is of two superimposed structures with 8-oxoG (magenta) determined here or undamaged G (yellow) (7) in the template base position. The DNA in the structures is similar and the 90° bend at the position of the template base 8-oxoG or G is evident (Fig. S2*B*). The different modeled conformations of the 8-oxoG nucleotide in the template base position are shown in the smaller circle. Also shown is a magnification illustrating different positions for the reference structure (yellow) and the three positions modeled for 8-oxoG in the template base position (see Fig. 1).

Properties of the preinsertion ternary complex structure with 8-oxoG in the template position and a nonhydrolyzable analog of dATP as the incoming nucleotide. As discussed in the main text and illustrated here in Fig. S3, the structure of the ternary complex with the nascent base pair *syn*-8-oxoG and *anti*-dATP revealed that the polymerase is in the closed conformation and similar to that of the reference structure (PDB ID code 2FMS) (Fig. S3*A*). The posi-

tion of the 5′-phosphate of *syn*-8-oxoG is similar to that observed for one of the conformations in the binary complex structure (Fig. S3*B*).

Preinsertion ternary complex structure with 8-oxoG in the template position and dCTP as the incoming nucleotide. To compare the results described above with error-free bypass of the 8-oxoG lesion, we determined the structure of a complex with templating 8-oxoG and incoming dCTP. We obtained this new preinsertion ternary complex structure of pol β with 8-oxoG in the template position by soaking the binary complex crystals with the nonhydrolyzable incoming nucleotide dCMP(CF_2)PP described above (Fig. 4). The primer terminus sugar contains the O3′. The crystal diffracted to 2.0 Å resolution (Table S2). The structure is similar to that previously reported (4) with an rmsd of 0.4 Å for all 325 Cα. The distance between the primer O3′ and Pα is 3.5 Å. The notable differences between this structure and the previous structure obtained with a dideoxy-terminated primer (8) may be summarized as follows: (*i*) the catalytic metal (Mg^{+2}) is present in the active site (Fig. 4*A*); and (*ii*) the Lys280 side chain that interacts with the templating 8-oxoG is altered (Fig. 4*C*). A survey of the various ternary complex structures of pol β revealed that the Lys280 side-chain is flexible and can adopt multiple conformations (Fig. S4).

In the new structure, to accommodate O8 in the *anti*-conformation the phosphate backbone rotates approximately 200° and moves 2.9 Å, compared to the reference structure (Fig. 4*B*) (PDB ID code 2FMS). Without an adjustment in the position of the backbone 5′-phosphate of 8-oxoG, a steric clash with the backbone would occur. Regarding any potential clash between O8 of 8-oxoG in the *anti*-conformation and O4′ of the sugar ring, the structure reveals that the corresponding distance is 3.3 Å. Evidently, the base-pairing and other interactions stabilizing the *anti*-conformation of 8-oxoG in the nascent base pair with C override any repulsion associated with this O4′ sugar ring proximity.

Primer extension from the mutagenic template-primer terminus. Another important feature in 8-oxoG-induced mutagenesis is extension off the *syn*-8-oxoG:*anti*-A Hoogsteen base pair and *anti*-8-oxoG:*anti*-C base pair at the template-primer terminus. This is relevant to long patch BER following insertion of dATP or dCTP opposite template 8-oxoG, because these base pairs would be positioned at the template-primer terminus in the gapped DNA substrate. Kinetic characterization of extension of 8-oxoG-containing base pairs is summarized in Table S3. Extension off the template-primer terminus combinations of 8-oxoG/A and 8-oxoG/C was similar to that for unmodified G/C and nearly 1,000 times more efficient than extension off the mismatched G/A terminus (Table S3), indicating that the mutagenic base pair (8-oxoG/A) is well accommodated at the template-primer terminus.

To gain insight on the structural basis for the efficient pol β extension off a template-primer terminus with the 8-oxoG:A base pair, we obtained the corresponding binary and ternary complex structures (Table S2); unmodified G was used in the template base position of the gapped DNA substrate. First, the binary complex crystal diffracted to 2.0 Å resolution, and the structure reveals that the enzyme is in the open conformation, as expected. The *syn*-8-oxoG:*anti*-A base pair is at the template-primer terminus (Fig. S5*A*). At this 8-oxoG position in the DNA strand, repositioning of the phosphodiester backbone is not required to accommodate the *syn*-conformation. Next, the ternary complex crystal structure with the 8-oxoG:A base pair at the template-primer terminus was examined (Table S2). The nascent base pair in the active site is G : dCMP(CF_2)PP. The structure reveals the *syn*-8-oxoG:*anti*-A Hoogsteen base pair at the template-primer terminus, and Arg283 stabilizes the *syn*-conformation of 8-oxoG through a hydrogen bond (3.27 Å) with O8. It is striking that the positions of O3′ and key active site atoms are very similar to those in the reference structure with an unmodified template-primer terminus base pair (Fig. S5*B*). Taken together, these structural results indicate that pol β accommodates the *syn*-8-oxoG:*anti*-A base pair at the template-primer terminus very well, and the structural results are consistent with the kinetic data in Table S3.

Structure of the complex with the anti-8-oxoG:anti-C base pair at the template-primer terminus. To provide context for the results described above, binary and ternary complex structures (Table S4) were obtained where the 8-oxoG:C combination is positioned at the template-primer terminus (n-1 position) and the template base in the adjacent single-nucleotide gapped DNA is an unmodified G. The structure of the binary complex (Fig. S6*A*) reveals that the Watson–Crick base pair *anti*-8-oxoG:*anti*-C is at the template-primer terminus, and this 8-oxoG:C base pair is indistinguishable from the reference structure with the unmodified G:C base pair, including the primer terminus sugar and position of O3′. The phosphodiester backbone adjustment observed when 8-oxoG is in the template base position is not relevant for 8-oxoG in the n-1 position and no adjustment is observed. A potential clash between the sugar oxygen (O4′) and O8 of 8-oxoG may not be strong, as the distance is 3.5 Å (not illustrated).

The structure of the corresponding ternary complex (Fig. S6*B*) with a nascent base pair in the active site (template base G and incoming dCMP(CF_2)PP) is similar to that observed with the reference structure (2) with unmodified template-primer terminus with rmsd of 0.2 Å for all 325 Cα (comparison not shown); the key active site amino acid side chains and primer terminus sugar O3′ are in similar positions (Fig. S6*B*). Arg283 is not within hydrogen bonding distance of O8 of *anti*-8-oxoG. In summary, placing the 8-oxoG:C base pair at the template-primer terminus results in a structure very similar to that with the unmodified G:C base pair in this position (Fig. S6*C*). These results suggest that the primer in the 8-oxoG:C base pair, when positioned at the template-primer terminus, will be readily extended by pol β, and this is consistent with the results from kinetic studies of the enzyme (Table S3).

Because the position of Lys280 relative to the template base is different in the structures determined here and an earlier structure obtained without the primer 3′-OH, we were curious to know whether the Lys280 position correlated with the presence of the primer 3′-OH. A survey of various pol β structures (already published and reported in this study) with or without the 3′-OH at the primer terminus revealed that the side-chain of Lys280 can adopt multiple conformations (Fig. S4); there was no correlation with the presence of the primer 3′-OH.

The 8-oxoG:C base pair at the n-1 position of BF polymerase also is observed in the *anti-anti*-conformation (9, 10). However, *anti*-8-oxoG induces an adjustment in the template strand so as to avoid a clash between O8 and O4′ of the sugar (11). This template strand adjustment is transmitted to altered minor groove interactions, preventing the adjacent template base from occupying the preinsertion active site. These alterations correlate with decreased BF enzymatic activity for the corresponding substrate with 8-oxoG at the template-primer terminus.

It is interesting to consider whether the specificity for error-free or error-prone 8-oxoG bypass by some of the polymerases, as summarized in Table S1, can be explained by different steps in the polymerase reaction cycle. For example, stabilizing the binary complex so that only one of the 8-oxoG base-pairing edges is presented to the incoming nucleotide, or stabilizing the nascent base pair in the ternary complex, may enhance the probability of nucleotidyl transfer. In the case of the Dpo4 polymerase, the binary complex structure with 8-oxoG in the template base position reveals stabilization of 8-oxoG in the *anti*-conformation through a network of multiple hydrogen bonds (11). This explains, at least in part, the remarkable specificity for error-free bypass of 8-oxoG by the Dpo4 polymerase. On the other hand, in the example of

the pol β where the enzyme exhibits similar efficiencies for dCTP and dATP insertion (Table S1), the binary complex active site provides for flexibility so that both conformations of the 8-oxoG base can be presented to an incoming dNTP. In addition, the ternary complex active site also provide for flexibility in the phosphodiester backbone so the both conformations of 8-oxoG can be accommodated.

1. Batra VK, et al. (2006) Magnesium-induced assembly of a complete DNA polymerase catalytic complex. *Structure* 14:757–766.
2. Otwinowski Z, Minor W (1997) Processing of X-ray diffraction data collected in oscillation mode. *Methods Enzymol* 276:307–326.
3. Pettersen EF, et al. (2004) UCSF Chimera—a visualization system for exploratory research and analysis. *J Comput Chem* 25:1605–1612.
4. Krahn JM, et al. (2003) Structure of DNA polymerase beta with the mutagenic DNA lesion 8-oxodeoxyguanine reveals structural insights into its coding potential. *Structure* 11:121–127.
5. Nishimura S (2006) 8-Hydroxyguanine: From its discovery in 1983 to the present status. *Proc Jpn Acad Ser B Phys Biol Sci* B 82:127–141.
6. Krahn JM, et al. (2003) Structure of DNA polymerase β with the mutagenic DNA lesion 8-oxodeoxyguanine reveals structural insights into its coding potential. *Structure* 11:121–127.
7. Michaels ML, Miller JH (1992) The GO system protects organisms from the mutagenic effect of the spontaneous lesion 8-hydroxyguanine (7,8-dihydro-8-oxoguanine). *J Bacteriol* 174:6321–6325.
8. Miller H, et al. (2000) 8-oxodGTP incorporation by DNA polymerase beta is modified by active-site residue Asn279. *Biochemistry* 39:1029–1033.
9. Brown JA, Duym WW, Fowler JD, Suo Z (2007) Single-turnover kinetic analysis of the mutagenic potential of 8-oxo-7,8-dihydro-2′-deoxyguanosine during gap-filling synthesis catalyzed by human DNA polymerases lambda and beta. *J Mol Biol* 367:1258–1269.
10. Hsu GW, Ober M, Carell T, Beese LS (2004) Error-prone replication of oxidatively damaged DNA by a high-fidelity DNA polymerase. *Nature* 431:217–221.
11. Pleasance ED, et al. (2010) A comprehensive catalogue of somatic mutations from a human cancer genome. *Nature* 463:191–196.

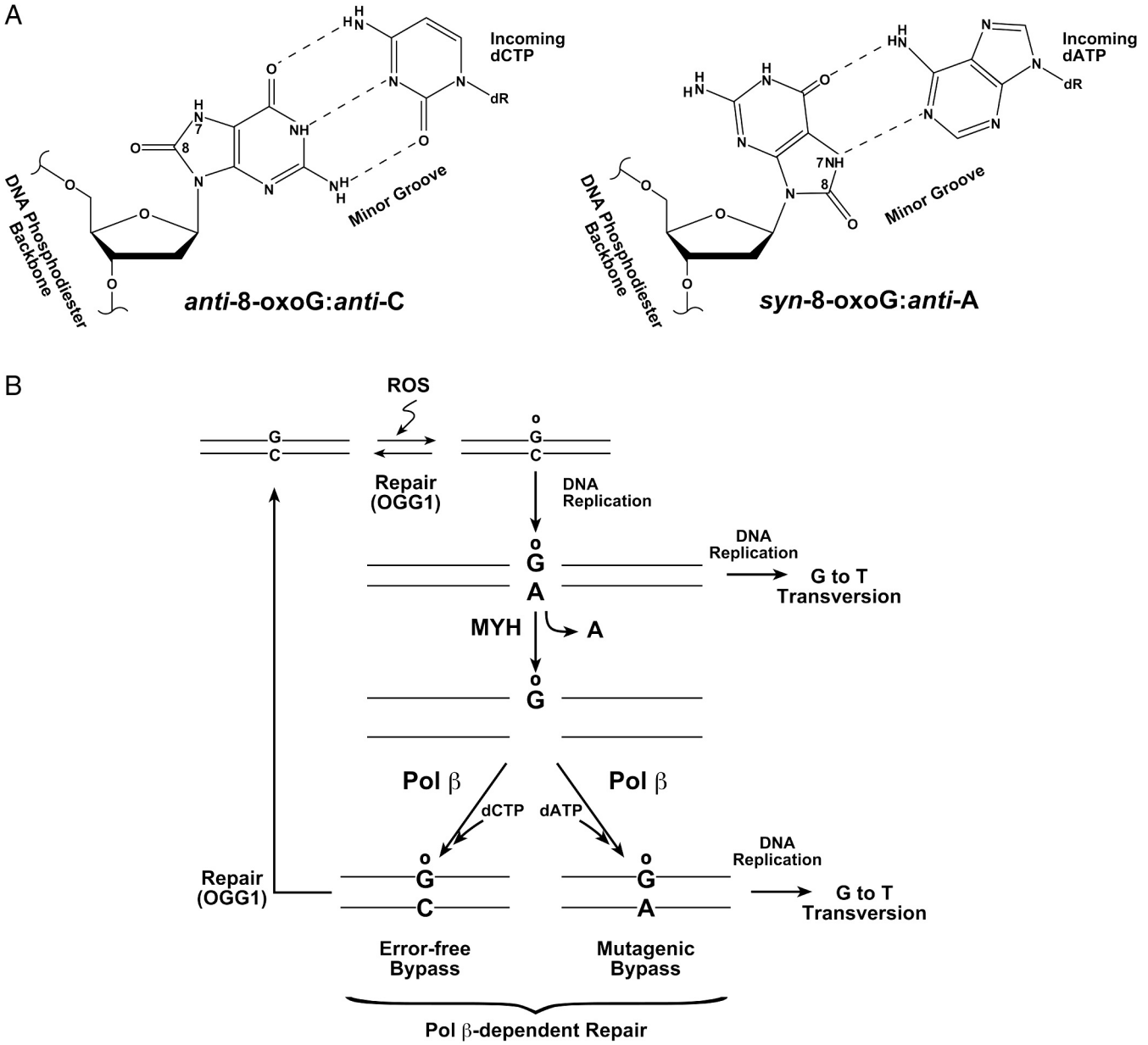

Fig. S1. Special features of the 8-oxoG base in the template base position. (*A*) Illustration of dual coding potential of template 8-oxoG in the nascent base pair binding pocket. In the *anti*-conformation, 8-oxoG forms a Watson–Crick base pair with cytosine. Oxidation at C8 of guanine also results in altered hydrogen bonding capacity of the Hoogsteen edge of guanine by converting N7 to a hydrogen bond donor that can base pair with adenine. Whereas the unmodified deoxyguanine glycosidic torsion angle (χ) preference is *anti*-, isolated 8-substituted purine nucleosides favor a *syn*-conformation due to steric repulsion be-

tween the deoxyribose and O8 of the modified purine base. The DNA minor groove and phosphodiester backbone are indicated. (*B*) Illustration of mutagenesis, DNA repair, and replication of 8-oxoG: A portion of the highly conserved GO system (5) that was first illuminated in *Escherichia coli*. The repair of the oxidized base, 8-oxoG, in DNA is initiated by a DNA damage-specific glycosylase. *E. coli* MutM or the human homolog OGG1, removing the 8-oxoG base paired with cytosine to purify the genome of the oxidized base. During DNA replication, unrepaired 8-oxoG can code for dCMP and dAMP incorporation. To remove a "misinserted" adenine, *E. coli* MutY or the human homolog MYH initiates BER by removing the mutagenic adenine base. In mammalian systems, DNA polymerase β gap-filling DNA synthesis will result in restoring the DNA substrate for either OGG1 (8-oxoG:C) or MYH (8oxoG:A). Replication of the unrepaired adenine-containing strand can result in the G to T transversion.

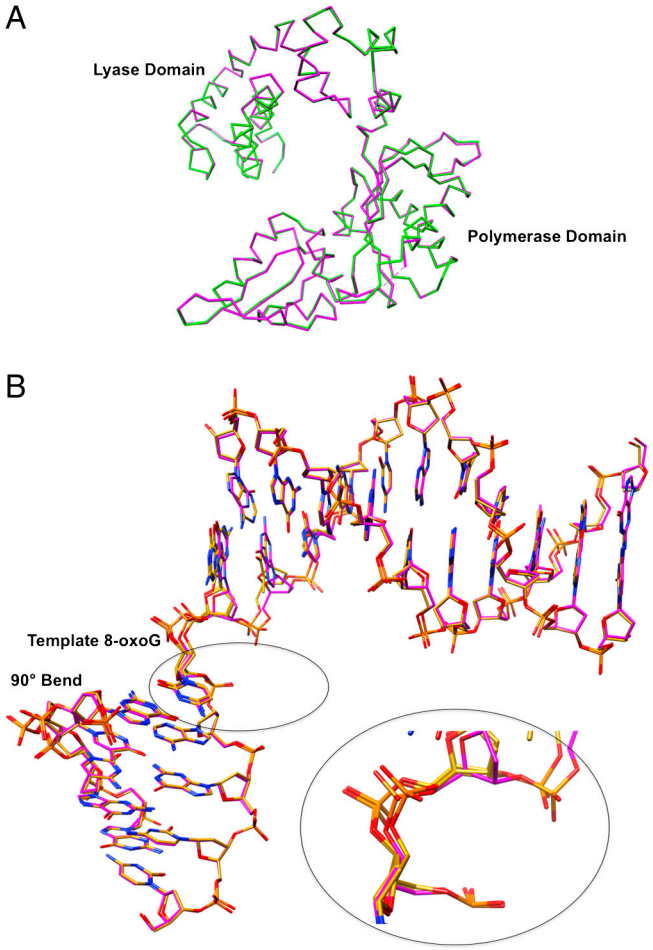

Fig. S2. Features of the human pol β binary complex structure with 8-oxoG in the template base position. (*A*) Superimposed stick representations of the Cα trace of the binary complexes of human pol β in the open conformation with 8-oxoG (magenta) and undamaged G (green) reference structure (PDB ID code 3ISB) as the template base. The two structures superimpose with rmsd of 0.2 Å for all 326 Cα. (*B*) Superimposed single-nucleotide gapped DNA with 8-oxoG (yellow carbons) or undamaged G (magenta carbons) in the template base position. The image illustrates the 90° bend in the template strand and that there are multiple conformations of the template 8-oxoG base. The 8-oxoG base is modeled in three conformations, as is the 5′-phosphodiester backbone; these conformations are illustrated in Fig. 1. The image in the larger circle is a magnified view of the conformations of the 5′-phosphate in the phosphodiester backbone.

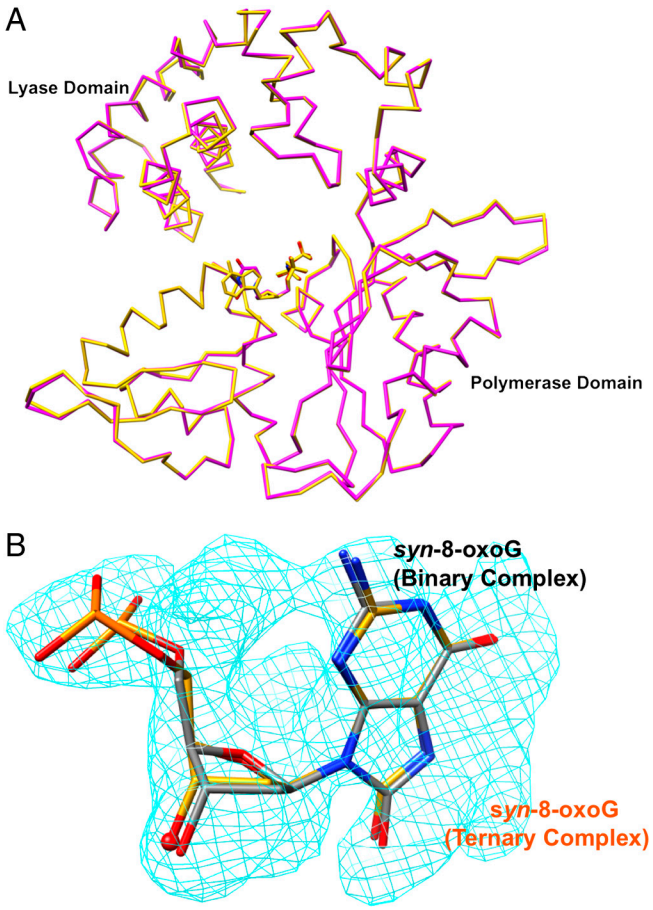

Fig. S3. Features of the human pol β ternary complex structure with 8-oxoG in the template position. (*A*) Superimposed stick representations of pol β backbone structures in two closed ternary substrate complexes. The backbone structure of pol β with template 8-oxoG and incoming dAMPCPP (gold) is superimposed with the reference pol β structure (1) with A in the template base position and incoming dUMPNPP (PDB ID code 2FMS) (magenta). The incoming dNTP in each structure is shown, but the DNA and metals are omitted for clarity. The two structures superimpose with rmsd of 0.3 Å for all 326 Cα. The results of this comparison indicate that α-Helix N is in the "closed" conformation in the structure of the template 8-oxoG containing complex. The amino-terminal lyase domain and α-helix N in the polymerase domain are indicated. (*B*) Illustration of the *syn*-conformation of 8-oxoG in the binary and ternary complex structures. The two template 8-oxoG nucleotide structures are superimposed.

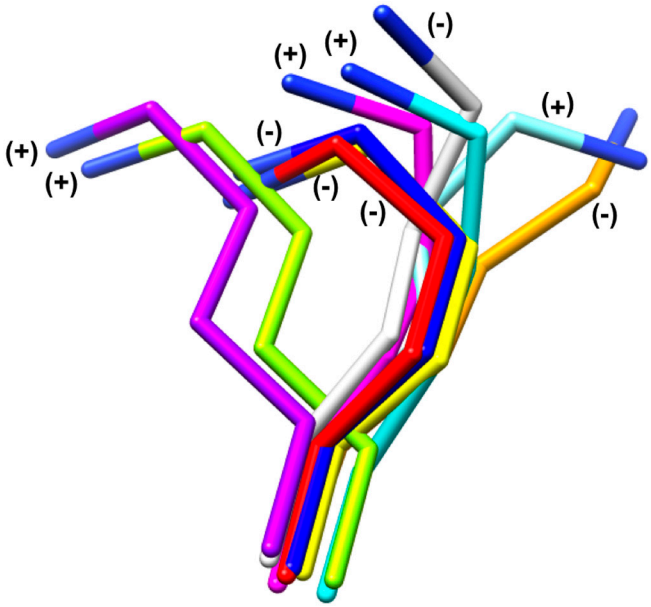

Fig. S4. Survey of conformations of Lys280 in pol β structures. The survey of various ternary complex structures of pol β with dideoxy-terminated primers [i.e., lacking 3′-OH (–) or with 3′-OH (+)] reveals that Lys280 can adopt multiple conformations in the active site. The position of Lys280 is not dependent on the presence or absence of 3′-OH. The following PDB files were used to illustrate the Lys280 conformations lacking 3′-OH: 2FMP (gray), 3MBY (yellow), 3JPO (blue), 3JPN (red), and 1MQ3 (gold). The following PDB files contain 3′-OH: 2FMS (maroon), 3LK9 (cyan), template 8-oxoG with an incoming dCMP(CF_2)PP (green) or an incoming dAMPCPP (magenta), and 8-oxoG:A base pair at the primer terminus with an incoming dCMP(CF_2)PP (light blue).

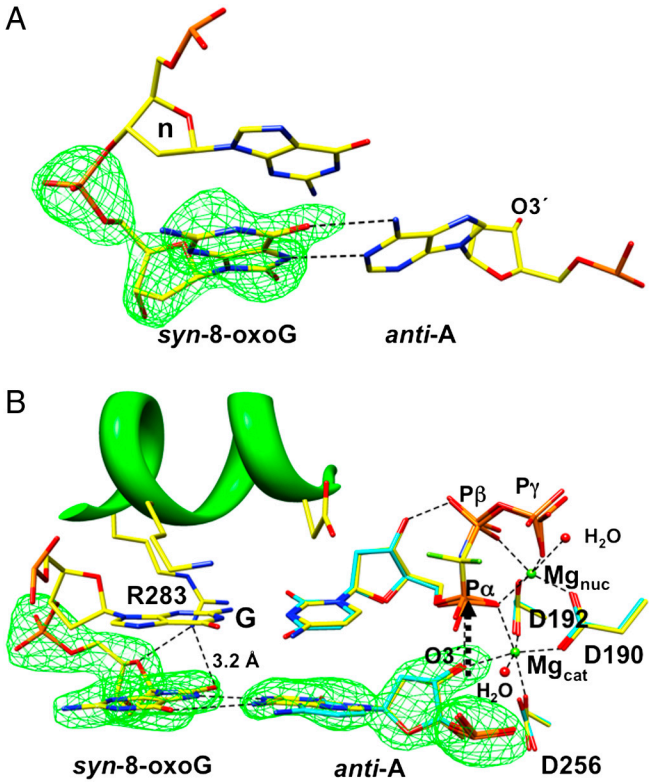

Fig. S5. Binary and ternary complex structures with the *syn*-8-oxoG:*anti*-A base pair at the template-primer terminus. (*A*) The open binary DNA complex with the *syn*-8-oxoG:*anti*-A Hoogsteen base pair observed at the template-primer terminus. The templating unpaired guanine nucleotide (n) and O3′ of the primer are indicated. An omit map (green) for *syn*-8-oxoG at the template-primer terminus contoured at 4σ is also shown. H-bonds are shown as dashed lines. *B*) In the closed ternary complex, the *syn*-8-oxoG:antiA base pair is at the template-primer terminus. The dG:dCMP(CF_2)PP base pair is in the nascent base pair binding site. Arg283 of α-helix N also stabilizes the *syn*-conformation of 8-oxoG through O8 and Nη1 hydrogen bond (3.2 Å) when the 8-oxoG containing base is at the n-1 position. This active site (cyan) resembles that with an undamaged base pair at the primer terminus (yellow) (PDB ID code 2FMS). The two active site magnesium ions (green spheres) and two coordinating water molecules (red spheres) are shown, along with coordinating oxygens from Asp 256 (D256), Asp 192 (D192), and Asp 190 (D190). The omit map (green) for the *syn*-8-oxoG:*anti*-A base pair contoured at 4σ is also shown. The O3′ to Pα distance is 3.4 Å (arrow).

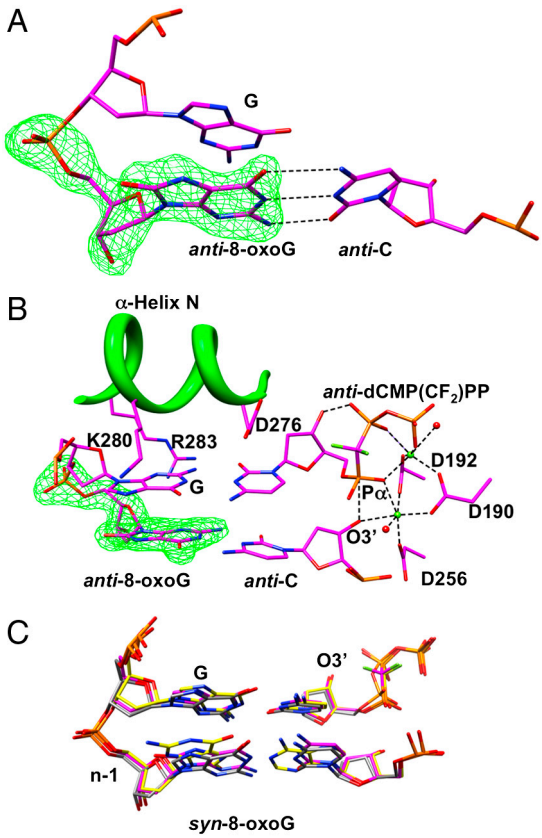

Fig. S6. Structures representing error-free extension of the 8-oxoG:C base pair at the template-primer terminus. The perspective is from the major groove. (*A*) Illustration of the template-primer terminus and the template base, G, in a portion of the active site of the open binary complex. An omit map of the 8-oxoG nucleotide in an *anti*-conformation contoured at 4σ is shown. (*B*) A detailed illustration of the structure of the pol β active site with the *anti*-8-oxoG:*anti*-C base pair at the template-primer terminus in the closed ternary complex. G in the template base position is paired with incoming dCMP(CF_2)PP, as shown. An omit map (green) for the *anti*- 8-oxoG base contoured at 4σ is also shown. Features of the active site illustrate that the fully assembled prechemistry active is present and the distance between the primer O3′ and Pα is 3.4 Å. The hydrogen bond between O3′ and the Pβ oxygen of the incoming nucleotide, similar to that seen in the reference structure, is illustrated. H-bonds are shown as dashed lines; metal coordination and O3′ to Pα distances are shown in dotted lines. (*C*) A superposition of three structures illustrating that 5′-phosphodiester backbone adjustment is not observed when 8-oxoG is positioned in the template strand at the template-primer terminus (n-1 position). The overlay of the reference structure with unmodified G (gray) and *anti*-8-oxoG (magenta) at the template-primer terminus illustrates lack of phosphodiester backbone adjustment. The structure with *syn*-8-oxoG (yellow) is also included in this overlay.

Table S1. Survey of reported DNA polymerase insertion efficiencies with 8-oxoG as the templating base

DNA polymerase * (family)	dCTP:dATP † insertion ratio	dCTP ‡ (8-oxoG/G)	References §
Dpo4 (Y)	61:1	27	1–3
Pol η (Y)	43:1	0.724	4, 5
RB69 (B)	20:1	0.022	6
Klenow (A)	6:1	0.221	7, 8
ϕ29 (B)	5:1	<0.001	9
T7 (A)	2:1	0.007	10
Pol β (X)	2:1	0.189	11, 12
Pol λ (X)	1:1	0.389	12
Pol ζ (B)	1:1	0.010	13
Pol δ (B)	1:1	0.043	14
Pol II (B)	1:1	0.003	7
Pol α (B)	1:7	0.018	8
Bacillus fragment (A)	1:9	<0.001	15
HIV1-RT (RT)	1:13	0.001	10
Pol κ (Y)	1:53	0.024	16–18

*Polymerases are listed in order of decreasing dCTP/dATP specificity.
†Ratio of insertion efficiencies with 8-oxoG as the templating base.
‡Ratio of dCTP insertion efficiencies opposite 8-oxoG and G.
§The average results are presented when more than a single study is reported.

1 Rechkoblit O, et al. (2009) Impact of conformational heterogeneity of OxoG lesions and their pairing partners on bypass fidelity by Y family polymerases. *Structure* 17:725–736.
2 Boiteux S, le Page F (2001) Repair of 8-oxoguanine and Ogg1-incised apurinic sites in a CHO cell line. *Prog Nucleic Acid Res Mol Biol* 68:95–105.
3 Nishimura S (2001) Mammalian Ogg1/Mmh gene plays a major role in repair of the 8-hydroxyguanine lesion in DNA. *Prog Nucleic Acid Res Mol Biol* 68:107–123.
4 Russo MT, et al. (2004) Accumulation of the oxidative base lesion 8-hydroxyguanine in DNA of tumor-prone mice defective in both the Myh and Ogg1 DNA glycosylases. *Cancer Res* 64:4411–4414.
5 Michaels ML, Miller JH (1992) The GO system protects organisms from the mutagenic effect of the spontaneous lesion 8-hydroxyguanine (7,8-dihydro-8-oxoguanine). *J Bacteriol* 174:6321–6325.
6 Feig DI, Reid TM, Loeb LA (1994) Reactive oxygen species in tumorigenesis. *Cancer Res* 54:1890s–1894s.
7 Meira LB, et al. (2008) DNA damage induced by chronic inflammation contributes to colon carcinogenesis in mice. *J Clin Invest* 118:2516–2525.
8 Tan X, Grollman AP, Shibutani S (1999) Comparison of the mutagenic properties of 8-oxo-7,8-dihydro-2′-deoxyadenosine and 8-oxo-7,8-dihydro-2′-deoxyguanosine DNA lesions in mammalian cells. *Carcinogenesis* 20:2287–2292.
9 Xie Y, et al. (2004) Deficiencies in mouse Myh and Ogg1 result in tumor predisposition and G to T mutations in codon 12 of the K-ras oncogene in lung tumors. *Cancer Res* 64:3096–3102.
10 Al-Tassan N, et al. (2002) Inherited variants of MYH associated with somatic G : C → T : A mutations in colorectal tumors. *Nat Genet* 30:227–232.
11 Uesugi S, Ikehara M (1977) Carbon-13 magnetic resonance spectra of 8-substituted purine nucleosides. Characteristic shifts for the syn conformation. *J Am Chem* 99:3250–3253.
12 Broyde S, et al. (2008) Lesion processing: High-fidelity versus lesion-bypass DNA polymerases. *Trends Biochem Sci* 33:209–219.
13 Lee W, et al. (2010) The mutation spectrum revealed by paired genome sequences from a lung cancer patient. *Nature* 465:473–477.
14 Pleasance ED, et al. (2010) A comprehensive catalogue of somatic mutations from a human cancer genome. *Nature* 463:191–196.
15 de Vega M, Salas M (2007) A highly conserved tyrosine residue of family B DNA polymerases contributes to dictate translesion synthesis past 8-oxo-7,8-dihydro-2′-deoxyguanosine. *Nucleic Acids Res* 35:5096–5107.
16 Maki H, Sekiguchi M (1992) MutT protein specifically hydrolyses a potent mutagenic substrate for DNA synthesis. *Nature* 355:273–275.
17 Nakabeppu Y (2001) Regulation of intracellular localization of human MTH1, OGG1, and MYH proteins for repair of oxidative DNA damage. *Prog Nucleic Acid Res Mol Biol* 68:75–94.
18 Batra VK, et al. (2010) Mutagenic conformation of 8-oxo-7,8-dihydro-2′-dGTP in the confines of a DNA polymerase active site. *Nat Struct Mol Biol* 17:889–890.

Table S2. Crystallographic statistics

	8-oxoG at template position			8-oxoG at n-1 position Primer terminus A	
Ligand	None	dAMP(CH_2)PP	dCMP(CF_2)PP	None	dCMP(CF_2)PP
Data collection					
Space group	$P2_1$	$P2_1$	$P2_1$	$P2_1$	$P2_1$
a (Å)	54.49	50.55	50.76	54.66	50.53
b (Å)	79.17	79.81	80.18	79.59	79.91
c (Å)	54.89	55.69	55.79	55.00	55.46
β (°)	105.58	107.88	107.96	105.79	108.04
d_{min} (Å)	2.10	2.30	2.10	2.00	2.20
R_{merge} (%) *, †	0.086 (0.255)	0.062 (0.337)	0.087 (0.430)	0.094 (0.358)	0.075 (0.361)
Completeness (%)	99.1 (93.7)	99.6 (98.6)	98.9 (91.7)	97.1 (91.5)	99.7 (100)
Unique reflections	25,984 (2,440)	18,697 (1,832)	24,662 (2,257)	29,866 (2,804)	21,352 (2,095)
Total reflections	86,259	67,096	87,708	106,660	74,229
I/σ	13.9 (3.27)	16.4 (3.09)	12.6 (2.29)	12.1 (3.14)	15.8 (3.21)
Refinement					
Rmsd					
Bond lengths (Å)	0.005	0.006	0.006	0.005	0.005
Bond angles (°)	1.101	1.066	1.076	1.057	1.078
R_{work} (%) ‡	19.81	19.32	22.01	20.76	20.39
R_{free} (%)	25.14	25.57	28.11	25.65	25.89
Average B factors (Å)					
Protein	25.17	34.57	30.40	24.40	31.76
DNA	24.54	44.94	44.05	26.40	39.89
8OG	49.07 (49.81)	32.76	30.85	39.04	27.00
Analogue	NA	21.13	15.39	NA	16.29
Ramachandaran analysis					
Favored	97.2	96.9	96.9	96.3	97.8
Allowed	99.4	100	99.7	99.3	100

*$R_{merge} = 100 \times \Sigma_h \Sigma_i ||_{h,i} - |_h| \Sigma_h \Sigma_i I_{h,j}$, where I_h is the mean intensity of symmetry related reflections $I_{h,j}$.
†Numbers in the parentheses refer to the highest resolution shell of data (10%).
‡$R_{work} = 100 \times \Sigma |F_{obs}| - |F_{calc}| / \Sigma |F_{obs}|$.

Table S3. Steady-state kinetic parameters for correct dCTP insertion on 8-oxoG modified template-primer termini

3′-terminus *	k_{cat}	K_m	k_{cat}/K_m	f_{ext} †
	10^{-2} (s^{-1})	(μM)	10^{-3} (s^{-1} μM^{-1})	
G-C	15.7 (0.8)	0.66 (0.04)	240 (20)	1.0
8-oxoG-C	12.7 (0.4)	0.21 (0.01)	620 (30)	0.4
G-A	1.5 (0.1)	57 (14)	0.26 (0.07)	920
8-oxoG-A	10.0 (0.7)	0.16 (0.02)	630 (90)	0.4

The results represent the mean (SE) of at least two independent determinations.
*The identity of the primer terminus is given as template nucleotide-primer nucleotide.
†The relative mispair extension efficiency is calculated from the ratio of catalytic efficiencies for correct dCTP insertion on a matched (i.e., G-C) and modified primer terminus (1).

1 Beard WA, Batra VK, Wilson SH (2010) DNA polymerase structure-based insight on the mutagenic properties of 8-oxoguanine. *Mutat Res* 703:18–23.

Table S4. Crystallographic statistics

	8-oxoG at n-1 position: C at terminus	
Incoming dNTP	None	dCMP(CF_2)PP
Data collection		
Space group	$P2_1$	$P2_1$
a (Å)	54.48	50.65
b (Å)	79.41	79.97
c (Å)	54.91	55.51
β (°)	105.51	107.55
d_{min} (Å)	2.00	2.10
R_{merge} (%)*, †	0.096 (0.343)	0.109 (0.370)
Completeness (%)	99.4 (98.3)	99.2 (93.4)
Unique reflections	30,356 (2,978)	24,479 (2,279)
Total reflections	108,909	84,915
I/σ	11.6 (3.04)	10.0 (2.63)
Refinement		
Rmsd		
Bond lengths (Å)	0.005	0.005
Bond angles (°)	1.055	1.110
R_{work} (%) ‡	20.15	19.94
R_{free} (%)	26.10	25.83
Average B factors (Å)		
Protein	19.41	21.87
DNA	20.89	29.25
8OG	22.81	15.95
Analogue	NA	11.67
Ramachandaran analysis		
Favored	96.3	97.8
Allowed	99.4	100

*$R_{merge} = 100 \times \Sigma_h \Sigma_i ||_{h,i}\text{-}|_h| \Sigma_h \Sigma_i I_{h,j}$, where I_h is the mean intensity of symmetry related reflections $I_{h,j}$.

†Numbers in the parentheses refer to the highest resolution shell of data (10%).

‡$R_{work} = 100 \times \Sigma |F_{obs}|\text{-}|F_{calc}| / \Sigma |F_{obs}|$.